STM JOURNALS

International Journal of
Satellite Remote Sensing

Volume 4, Issue 1, 2026
January–June
DOI (Journal): 10.37591/IJSRS

https://journals.stmjournals.com/ijsrs

Review IJSRS

Time Multiplexed Binary Offset Carrier (TMBOC) Transmitter with Polarimetric Interferometric Synthetic Aperture Radar (Pol-InSAR)

Sayanti Dutta[1], Raisa Chatterjee[2], Tamesh Halder[3,*], Rintu Kumar Gayen[1], Debashish Chakravarty[3]

Abstract

This paper provides insights into Time Multiplexed Binary Offset Carrier (TMBOC), a modulation technique employed in satellite navigation systems, specifically designed for GPS L1C. TMBOC improves signal correlation properties by time-multiplexing Binary Offset Carrier (BOC) (1, 1) and (6, 1). The text discusses various TMBOC models, including spectral representations and power distributions. Performance analysis reveals the potential of TMBOC signals in achieving superior tracking accuracy and interference resistance compared to other modulation techniques. Spectrum allocation considerations for TMBOC in the GPS L1 band are addressed. The information underscores the significance of TMBOC in enhancing the robustness and precision of satellite navigation systems, contributing to the continual evolution of signal modulation strategies in this technological domain. The literature on PolInSAR and PolSAR assesses the various techniques for estimating the forest height, biomass, and complex coherence. The study involves complex Wishart distribution-based methods and target decomposition-based methods. These techniques have the potency to demonstrate and retrieve the vegetation parameters and perform various land cover-based classifications. The images taken by radar have to be linked with GPS co-ordinates and ground control points for making digital surface model (DSM). This work is done at base stations while the GPS signals and images are received at master control units (MCU). Hence the thorough study and simulation of current state of arts in navigation paves the way of geographic-information systems (GIS) with remote sensing. The article bridge the GPS of current era modulation technique TMBOC and radar image Polarimetric Interferometric Synthetic Aperture Radar (Pol-InSAR).

Keywords: Time multiplexed binary offset carrier (TMBOC), spectral representations, GPS L1 band, signal correlation, signal modulation, spectrum allocation, PolSAR, Pol-InSAR, vegetation height determination, RVoG

***Author for Correspondence**
Tamesh Halder
E-mail: haldertamesh@iitkgp.ac.in

[1]Student, Department of Electronics and Communication Engineering Institute of Engineering & Management, Kolkata, India
[2]Student, Department of Electrical Engineering, Jadavpur University, Kolkata, India
[3]Professor, Department of Mining Engineering Indian Institute of Technology, Kharagpur, India

Received Date: March 17, 2026
Accepted Date: March 18, 2026
Published Date: May 16, 2026

Citation: Sayanti Dutta, Raisa Chatterjee, Tamesh Halder, Rintu Kumar Gayen, Debashish Chakravarty. Time Multiplexed Binary Offset Carrier (TMBOC) Transmitter with Polarimetric Interferometric Synthetic Aperture Radar (Pol-InSAR). International Journal of Satellite Remote Sensing. 2026; 4(1): 34–49p.

INTRODUCTION

This paper unfolds the narrative of navigation technologies, spanning from historical methods to contemporary systems. It places a significant emphasis on Binary Offset Carrier (BOC), Multiplexed Binary Offset Carrier (MBOC), and Time Multiplexed Binary Offset Carrier (TMBOC) modulation techniques. Beginning with an overview of ancient navigation practices, the chapter progresses to explore the working principles of modern navigation technologies. It delves into the intricacies of frequency plans and signal structures tailored for navigation applications. A focal point is the comprehensive analysis of BOC, MBOC, and TMBOC modulation techniques, showcasing their performance and significance in positioning systems. The chapter further discusses frequency band allocations linked to these modulation techniques. Practical aspects, including the implementation of MBOC communication systems, radio-navigational channel models, and the design nuances of MBOC transmitters and receivers, are elaborated. The chapter concludes by emphasizing the delicate balance between system performance and the evolving complexities of receiver technologies, shedding light on the ongoing optimization efforts in the field.

Pol-InSAR is an advanced technique that deploys the functionalities of the two SAR technologies, namely Polarimetric SAR (PolSAR) and Interferometric SAR (InSAR). These are potent techniques for topographic mapping on both regional and global scales. These are known for their high accuracy, end-to-end coverage, high resolution, and ability to perform in all weather conditions [1, 2]. InSAR detects the vertical forest structure and sub-canopy ground surface, thereby transcending other classical methods in terms of the underlying topography [3, 4]. A given target is illuminated by two SAR sensors at two different InSAR angles. Subsequently, elevation is measured by interferometric processing of master and slave SAR images [5]. The observation space is expanded from a single polarization channel to a dual or full-polarization channel (HH, HV, VH, VV) in PolSAR. PolSAR can characterize different scattering mechanisms and distinguish among different target units. Satellite Remote sensing is being increasingly used to provide wide-area estimates of the biomass content of forest regions. It is necessary to improve the coverage, resolution, and accuracy of global forest biomass baseline information to determine the accuracy and spatial resolution of above-ground biomass estimates.

We consider forest height as the key parameter for the evaluation of forest growth and site quality. This is an important factor for calculating biomass and carbon reserves [6,7]. Apart from Pol-InSAR, Light Detection and Ranging (LiDAR) and optical remote sensing have come up as the current state-of-the-art for forest height estimation. Cloude and Papathanassiou pioneered Pol-InSAR, which depends on the strong reliance of the interferometric phase on polarization [8]. Pol-InSAR is highly valuable method in characterization of vegetation [9, 10], generation of digital elevation model (DEM) [11, 12] and classification of landscapes [13, 14]. SAR polarimetry has been utilized in ESA and other missions like Terrasar, Radarsat 2, Alos Pulsar, SarVision, and Vexcel UK to assess applications like agriculture, land use classification, sea ice monitoring, etc. [15].

One major problem in Pol-InSAR is the selection of homogeneous pixels wherein the central pixel value is estimated through the Lee estimator. This is an unstable technique and crates a performance limit. To overcome this problem, an improved method of d-Pol-InSAR is proposed. This technique is based on complex coherence non- local estimation. A shape-adaptive patch is used in the region growing algorithm and likelihood ratio test to match similar pixels. Deployment of trace-moment-based non-local reduced bias estimator utilizing Wishart distribution yields accurate homogeneity results for the selected pixels by considering inter-channel correlation [16]. The relationship between various polarization states and the phase distortion in Pol-InSAR is analyzed to interpret the detection mechanism of point targets. Few optimization methods i.e., Pixel-by-Pixel Optimization and Pixel-by-Pixel Optimization Considering Baseline Difference have been proposed in Pol-InSAR. These use high-resolution SAR data obtained from Advanced Land Observing Satellite-2 (ALOS-2) of the Japan Aerospace Exploration Agency [17]. Forest height inversion technique at P-band is implemented by collecting high-resolution data over pine forest located near Arcachon in Gironde (Landes, France).

This is done by the airborne RAMSES system in the “Pyla 2004” campaign during two different flights. The various characteristics of P- band Pol-InSAR data are: mean incidence angle around 45◦, resolution in the order of 3 m, ambiguity height is around 45 m which is variable due to changing spatial separation of the successive flight lines, and airborne acquisition [18]. The three different models for estimation of height using Pol-InSAR data are Random Volume over the Ground model (RVoG), Elevated Random Volume over Ground model (ERVoG), and Oriented Volume over the Ground model (OVoG) [4,19,20]. The use of repeat-pass Pol-InSAR over forests gives rise to de- correlation even over very short intervals. This leads to poor results, especially at L-Band. L-Band finds application because of its high forest penetration power and lesser bandwidth licensing restriction than the longer wavelength.

This paper is inspired by vast PolInSAR and LiDAR data that will be available from future missions like ESA's P-band SAR BIOMASS in 2021 [21], the joint NASA-ISRO L-band SAR (NISAR) in 2021 [22], and DLR's Tandem-L with Pol-InSAR L-band capabilities in 2023 [23]. Compared to Pol-InSAR, only merged height, overestimation of the height over sparse vegetation (5m), and underestimation over the tall vegetation has been reduced (∼10 m).

There are two major techniques followed in this work for the Pol-InSAR study. These are section 2.1 coherence added features in polarimetric decomposition and section 2.2 Volume scattering model estimation. These are discussed next.

METHODOLOGY

Firstly, we discuss how interferometric coherence adds more features in Pol-SAR [24] decomposition. Subsequently, we discuss volume scattering for forest height estimation, which is also an application of Pol-InSAR.

Coherence added features in POLSAR decomposition:

Sometimes, polarimetric decomposition generates negative power values causing misinterpretation of the oriented and highly dense buildings as volume scatterers instead of the dominant double-bounce scatterers. These classification models lead to overestimation of volume scattering and erroneous classification. A case study is done in Uttarakhand, India using the RADARSAT-2 dataset [25]. A statistical threshold parameter is considered in the decomposition model where a higher value indicates volume scattering and a lower one indicates the double-bound scattering. This parameter makes the model workflow dynamic and suitable for different imaging frequencies. It solves the problem of scattering ambiguity without underestimating or overestimating other decomposed scattering powers. It is shown that this model serves as a potential tool for applications in disaster management, rapid change detection, glacial studies, and deformation studies. The main goal is to differentiate two observable instances [26]. It has been shown from the polarimetric analysis that X-band is well adapted to remote vegetation sensing, providing good discrimination between different agricultural fields and trees. This is associated with the size of relevant scatterers having expected dimensions in the order of the wavelength. Examples include leaves-branches and grass fields. As a consequence, X-band is a good observation region to follow the different phenological stages of the vegetation. This high-resolution dataset indicates that X-band data could be useful for characterizing urban target types (electric poles, buildings). The complexity of the scattering occurring in some build-up areas with a strong multiple scattering component requires the simultaneous analysis of the full Pol-InSAR signature to provide a valid interpretation. A better separation in the complex coherence plane associated with different polarizations could be improved by selecting a longer baseline to decrease the height ambiguity and increase the sensitivity to differential penetration [27].

Tree height measurements given by InSAR, change over time and are hugely affected by intrinsic phase noise. This is due to the unstable canopy and dielectric properties of the ground. An InSAR system does not maintain temporal consistency because of the target phase noise. This ranges from slightly below the ground level to slightly above the true tree height. It depends on a multi-temporal combination and canopy enclosure. However, for retrieving the total true height from InSAR tree height measurements, attenuation and volume decorrelation compensations are necessary [28]. Temporal climatic variations related to CO2 emissions are used for biomass estimation. This can be inferred from tomographic images of the canopy in the forest. Pol-InSAR techniques are unable to retrieve the forest structure directly. In this paper, PolInSAR is combined with tomography to infer the biomass estimates of heterogeneous forest types [29]. "Standard" tomography requires multiple baselines from multiple passes leading to a rise in operational costs. To overcome this for airborne systems, Polarization

Coherence Tomography has been developed. This technique resolves the problem of the vertical distribution of scattering using fewer baselines. This method also tackles the issue of generating tomograms to highlight the possible interactions with biomass content.

A large number of good algorithms for the estimation of Pol-InSAR complex coherence have been reported. These include an extension of the Refined Lee speckle filter [30], a spatially adaptive filtering algorithm. Most of the other algorithms are based on various decomposition and classification schemes [31]. A similarity test has been applied for the determination of similar pixels (Simi Test Method). The test is implemented in a large 15 x 15 searching area associated with a nonlocal filtering concept [32]. InSAR generates phase differences between two complex-valued data of coherence. The remainder of the land height is divided by geometric parameters. This yields the phase value corresponding to each pixel since the phase difference corresponds to a change in heights. Unwrapping of folded phase images leads to the generation of DEM. The estimated height is dependent on the integration path. Consequently, singular points bring difficulty in DEM generation. The total length of branch-cuts [33] needs to be minimized since it results in artificial cliffs, which is a costly process. This problem is solved using unwrapping methods [34, 35], filtering methods [36, 37], local registration methods [38, 39], and methods using Pol-InSAR [40].

The distribution of the individual targets is unknown and too complex to be imitated. Consequently, a statistical characterization of the target's response is necessary and speckle is usually considered as a noise component. Therefore, pixel-based processing of SAR data has limitations due to this noise component. The limitation of the classical approach is overcome by considering Binary Partition Tree (BPT) data abstraction. A BPT may be considered as a region-based and multi-scale representation [41]. In the case of region-based representation, each node is created by merging two child nodes representing connected regions of the data. Root nodes represent the whole data set while individual pixels are represented by the leaves of the tree. There are many regions among the leaves and root nodes in the case of multi-scale abstraction. These denote areas of the scene having similar properties at different detail levels. BPT must be constructed from original data and then exploited through a pruning process performed by a top-down pruning algorithm. Initially, nodes having relative MSE below the threshold are extracted. Temporally fixed spatial contours are detected using an extended covariance matrix. It induces two-dimensional segmentation of data as it cannot adapt to the time-varying spatial contours. Thus, polarimetric, interferometric information, and spatial resolution are preserved by Binary Partition tree representation. The polarimetric properties have been described in terms of co-polar and cross-polar response diagrams for natural objects [42]. Lee et al. described the statistical variation of the amplitudes of the covariance matrix elements for polarimetric data by using Wishart distribution, have [43].

Volume Scattering Model Estimation

Two scenes of SAR images compose Pol-InSAR data. The vertical wavenumber of the data is determined by spatial baseline, incident angle, slant distance, and wavelength of the two images. There is a significant difference in the effect of inversion for different vertical wavenumbers in the Pol-InSAR data. The role of vertical wavenumber on the inversion effect has been studied to improve forest height inversion accuracy. There has been a setup of 39 groups of simulated data and 8 groups of fully polarized real P band E- SAR data with vertical wavenumbers ranging from 0.01 to 0.26. This setup avoids the interference of decoherence factor and speckle noise for the coniferous forest with heights of 10m, 15m, and 20m.

Random-Volume-Over-Ground (RVoG) model has been utilized for forest height inversion. The Remington area, located in southern Sweden containing tree species Pinus sylvestris and Picea abies and having forest height of 24 m, has been the study site. Interference coherence has been the basis of inversion by Pol-InSAR [44]. The ratio of the coherence matrix range decreases with an increase in vertical wavenumber and linearity gradually decreased for vertical wavenumber between 0.06 and 0.23. A limit between 0.06 and 0.10 has been the optimal vertical wavenumber interval of forest height inversion resulting in an inversion error of less than 15%.

Sparse low vegetation denotes generally high coherences and low phase-center heights. Reduced coherence in higher forests generally occurs due to volume decorrelation. The mean extinction coefficient is a function of the forest height, which is also linked to the tree density. The time-frequency method of Sub-look decomposition has been followed to separate the pure contributions of ground and canopy so that the forest height under OVoG assumptions is inverted with an RMS error of order 2m [45]. SNR and spatial resolution are studied as their influence on inversion has been variable while evaluating parameter extraction capabilities using P-band space-borne systems. It is observed that a reduction of SNR could induce overestimation of height by assuming unbiased ground level estimation. This can be corrected provided the quality of system evaluation is accurate. The SNR effect depends on the mean extinction coefficient and is set to a standard of 0.5dB/m. The various levels of SNR have been simulated in association with low- extinction random volume with a height ranging from 0 to 30 m. The height is compared with the unbiased value as derived from volume interferometric coherence. The ground-level estimation is affected by decreasing coherence in the RVoG inversion method. This influences the accuracy of height estimation. Two independent processes are used for estimating the resolution degradation process. These are spatial averaging and spectral filtering. Degradation of resolution affects the result of time-frequency inversion and supervised methods are seen to be more adaptive to space-borne data [46].

Model of man-made target beneath the foliage devises a multi-layer random scattering model. This model can be used for parameter inversion of the forest area containing such a man-made target [47].

Application to Underlying Topography Estimation introduces cancellation of scattering mechanisms [48]. It inspects the polarimetric dependence of the complex interferometric coherence. Based on the RVoG model, the projection vectors leading to a cancellation of the volume scattering or the ground scattering have been determined. They are compensated by because pairs of the coherency matrix elements include the polarimetric phase information with the opposite signs whereas the interferometric phase information is captured in elements with the same signs. By observing this, expressions for the simple and effective estimation for underlying vegetation and forest regions are derived. In addition to this, an expression for the phase linked with the volume decorrelation term is also determined. Thus, the utility of different polarization projection vectors to derive the complex interferometric coherence has been described in this paper [48].

Here we discussed about renown modulation schemes in navigation systems i.e. Binary Phase Shift Keying (BPSK), Binary Offset Carrier (BOC) and various types of Multiplexed Binary Offset Carrier (MBOC). Next their theoretical performance analysis is done with respect to Cramer Rao Lower Bound (CRLB). We also sketch their Power Spectral Density (PSD) according to the allocated spectrum. Furthermore, we compared the tracking errors of various modulation schemes namely BPSK, BOC and MBOC in section 2.5. To prove the supremacy of MBOC signals we relied on a hypothetical evaluation of CRLB criteria.

Modulation techniques

One of the navigation signal components is one or more spreading sequence(s), which is (are) modulated on a carrier signal. Each navigation signal has certain spreading codes and data which are modulated on the same carrier [49]. The spreading code of a signal signifies a unique Pseudo Random Noise (with binary level ±1), assigned to only one satellite. If the high-rate PRN code modulates the signal, the signal bandwidth becomes wider. For this reason, the PRN code is named as spreading code. The minimum time interval of transition in spreading code is called chip duration Tc. Generally, PRN sequences are Gaussian noise.

$$\frac{1}{N_{chip}}\sum_{i=1}^{N_{chip}} C_i C_{i+n} = \begin{cases} 1 & n = 0 \\ 0 & n \neq 0 \end{cases}$$

The product of PRN code and the sub carrier {C (t) x (t)} is known as Direct Sequence Spread Spectrum (DSSS). As we have already discussed signal structures, we emphasize the advantages and disadvantages of some modulation techniques as well as the supremacy of Multiplexed Binary Offset Carrier (MBOC) modulation over several modulations.

$$\sum_{i=1}^{N_{chip}} C_i C_i = 0$$

Where C_i is different satellite's PRN code.

Binary Phase Shift Keying (BPSK)

BPSK signal [55] is defined as a sinusoidal carrier modulated by a bipolar bit stream. BPSK (n) has center frequency n. 1.023 MHz. and it is defined as follows.

$$S_{BPSK}(t) \sum_{n=0}^{N_{chip}{}^{-1}} C_n Rec\left\{\frac{t - nT_c}{T_c}\right\}$$

Where Nchips is the number of chips present in one period of spreading code, Cn =C(nTn) is the code sign of the nth chip and

$$Rectangular\ pulse, Rec\left\{\frac{t}{T}\right\} = \begin{cases} 1 & |t| \leq \frac{T}{2} \\ 0 & otherwise \end{cases}$$

The Fourier transform of this signal is

$$S_{BPSK}(t) \sum_{n=0}^{N_{chip}{}^{-1}} C_n T_c sinc\ (fT_c) e^{-2i\pi T_c f n}$$

$$G_{BPSK}(f) \sum_{1=-(N_{chip}{}^{-1})}^{N_{chip}{}^{-1}} C_1 sinc^2\ (fT_c) e^{-2i\pi T_c f l}$$

$$G_{BPSK}(f) \sum_{n=0}^{N_{chips}{}^{-1}} \sum_{k=0}^{N_{chips}{}^{-1}} C_n T_c^2 sinc^2(fT_c) C_k e^{-2i\pi T_c f(\,n-k)}$$

The Power Spectral Density (PSD) of BPSK signal is

$$G_{BPSK}(t) = N_{chips} T_c \Delta(\frac{t}{T_C})$$

Where

$$\Delta(\frac{t}{T_C}) = \begin{cases} 1 & -\frac{1}{T}|t| \leq T \\ 0 & otherwise \end{cases}$$

$f_l > 0$ then $C_l = 0$ and if l = 0 then C_l = signum(Nchips). The Auto-Correlation Function of BPSK signal is denotes a triangular pulse.

Binary Offset Carrier (BOC)

A BOC signal comprises a Navigation data, PRN code, a sub-carrier and a sinusoidal carrier [49]. The BOC modulated signal is the product of these above said components in the time domain. BOC signal is referred to as BOC (m, n) or BOC (fs,fc) where fs = m x 1.023 MHz and fc = n x 1.023 MHz. The sub-carrier waveform and the PRN code bear direct relevance to the appearance of the BOC signal; hence proper assessment of the former is required for ensuring quality of the BOC signal. As the sinusoidal carrier is continuous, it doesn't contribute to any phase jump in the modulated signal. Since the Navigation data rate (50 bps for GPS, 250 bps for GALILEO) is far lower than the other components of signal, the priority is given to subcarrier signal and PRN code design. Now, the BOC signals can be defined in two ways.

1. Architecture using whole code sequence for one epoch: The sub-carrier which is equal to the signum of sine or cosine waveform is multiplied with the PRN code and it causes sine-phased BOC signal and cosine phased BOC signal (Figure 1).

   $S(t) = c(t)\text{signum}(\sin(2\pi\, fs\, t))$

   Where,
   $c(t) = \sum_k ckh(t - kTc)$ and ck is code waveform and h(t) is NRZ code.

2. Architecture using code sequence for one time interval: The second form $S(t) = \sum_k CkPTc(t-kTc)$ where PTc(t) denotes the chip waveform and is broken-up into n rectangular pulses of duration Tc/n with amplitude of 1. Now in this case the time series is shown in Figure 1 with Figure 2 we can clearly say that there are polarity inversion as every two bits in code sequence is same.

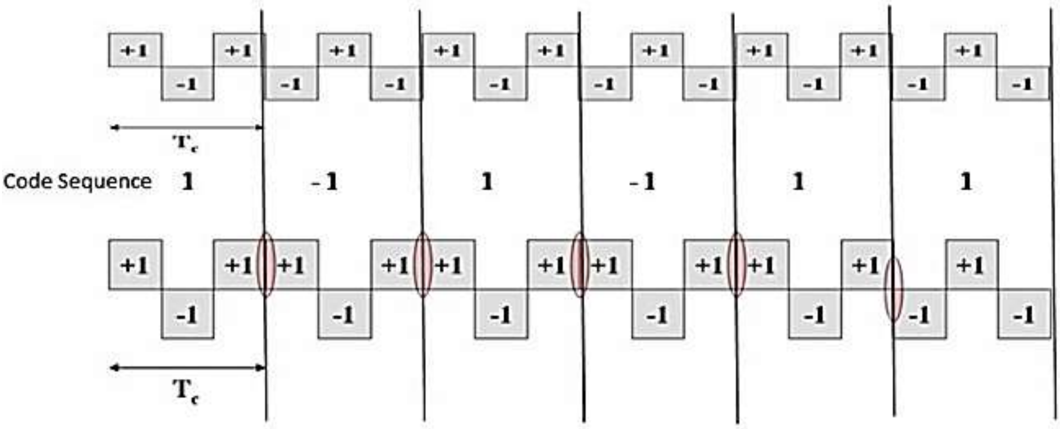

Figure 1. Sine phased Subcarrier (fs) [upper] Product of the sub-carrier and the code sequence (1,-1, 1,-1, 1, 1) in cases 1 and phase transition marked [lower].

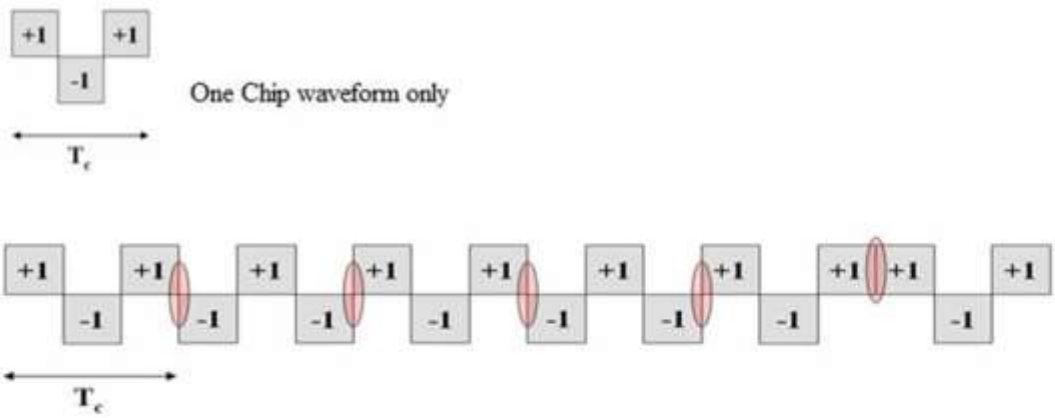

Figure 2. Product of the sine-phased chip waveform and the sequence (1,-1, 1,-1, 1, 1) in case 2.

Depending upon the adaptation in receiver architecture, we use either case 1 or case 2 to generate BOC signal conventionally. Now for 2nd cases when φ = 2 f s/ f c = 2m/n is odd, we modify chip waveform to include the subcarrier waveform properly.

$$S(t) = \sum_{K} (-1)^K CkpT_c\,(t - KT_c)$$

$$f_c = \frac{1}{\emptyset T_s} = \frac{2}{\emptyset} fs$$

We can easily derive the PSD of the sine subcarrier based BOC signal

$$G_e^{\sin BOC}(f) = \frac{1}{\phi T_S}\left[\frac{\sin^2\left(\frac{\pi f}{f_c}\right)\sin^2\left(\frac{\pi f}{\phi J_c}\right)}{\cos^2\left(\frac{\pi f}{\phi f}\right)(\pi f)^2}\right]$$

$$G_{MOD}^{BPSK(\phi f)}(f) = \frac{1}{\phi T_S}\cdot\frac{\sin^2\left(\frac{\pi f}{\phi f_c}\right)}{(\pi f)^2}$$

So, we say that,

$$G_e^{\sec BOC}(\mathrm{f}) = G_{MOD}^{\mathrm{BPSK}(\phi f_c)}(f)\cdot G_{MOD}^{\mathrm{e,\ \sin}BOC}(f)$$

In BOC signal there are four combinations of signal modulation.

Sine phased BOC with ϕ even. $G_{MOD}^{e,sinBOC}(f) = \frac{sin^2\left(\frac{\pi f}{f_c}\right)}{cos^2\left(\frac{\pi f}{\phi f_c}\right)}$

Sine phased BOC with ϕ odd. $G_{MOD}^{o,sinBOC}(f) = \frac{cos^2\left(\frac{\pi f}{f_c}\right)}{cos^2\left(\frac{\pi f}{\phi f_c}\right)}$

Cosine Phased BOC with ϕ even. $G_{MOD}^{e,cos\,BOC}(f) = \frac{4sin^2\left(\frac{\pi f}{f_c}\right)sin^2\left(\frac{\pi f}{\phi f_c}\right)}{cos^2\left(\frac{\pi f}{\phi f_c}\right)}$

Cosine Phased BOC with ϕ odd. $G_{MOD}^{o,cos\,BOC}(f) = \frac{4cos^2\left(\frac{\pi f}{f_c}\right)sin^2\left(\frac{\pi f}{\phi f_c}\right)}{cos^2\left(\frac{\pi f}{\phi f_c}\right)}$

We used the sine phased BOC (sine BOC) signal to create the MBOC signal in the transmitter. For a carrier to noise ratio of 41 dB-Hz, the search probability of a cosine phased BOC (cos BOC) signal is 50.4%, and the search probability of a sine phased BOC signal is 58.2%[56]. Band limiting has a greater impact on cosine phased signals, and the cosine-phased BOC autocorrelation form is thinner. The spectral energy is farther from the band center in the cosine signal because it has a higher proportion of high frequency, or higher side lobes that are positioned in between the major lobes in the spectrum. As shown, filtering has a greater effect on cosine signals than sine signals, which lowers the likelihood of detection. Thus, we might infer that there is a decreased chance of a successful search for cosine phased BOC signals.

Multiplexed Binary Offset Carrier (MBOC)

The result of adding or multiplexing two or more BOC signals is a modulated signal known as a multiplexed binary offset carrier (MBOC) [49]. For instance, narrowband BOC (1, 1) and wideband BOC (6, 1) make up MBOC (6, 1, 1/11). BOC (1, 1) has a different power level than BOC (6, 1). A common notation is MBOC(6,1,1/11), in which the modulation of BOC(6,1) is denoted by the word

(6,1) and the distribution of BOC(6,1) power spectral densities is represented by the ratio of 1/11. The data-conveying signal in MBOC notation is BOC (1,1), and the numerical terms represent the sub-carrier, sinusoidal carrier, and power distribution of the pilot signal. At higher frequencies, the BOC(6,1) subcarrier contributes a greater amount of energy than the BOC(1,1) sub-carrier that leads to a signal with sharper correlation function and thus gives the best performances in positioning the receiver. The MBOC normalized Power Spectral Density (PSD) is

$$G_{MBOC\left(6,1,\frac{1}{\pi}\right)}(f) = \frac{10}{11} G_{BOC(1,1)}(f) + \frac{1}{11} G_{BOC(6,1)}(f) \quad (1)$$

Types of MBOC

MBOC has many versions [50, 51]. Among them; the most popular ones are

1. Composite Binary Offset Carrier (CBOC) [E1 band]
2. Time Multiplexed Binary Offset Carrier (TMBOC) [E1 band]
3. Alternative Binary Offset Carrier (Alt-BOC) [E5 band]

Here we will limit our discussion to CBOC and TMBOC because of our interest in E1 band (E1 being used for navigation as discussed later). It is to be noted that Variable Binary Offset Carrier (VBOC) [52] has better tracking performance, multipath mitigation and it is more resilient to noise than MBOC modulation, yet this modulation technique does not get deployed by any of major navigation systems.

TMBOC

It is a GPS L1C solution. When the effect of the PRN code is taken into consideration, the binary signal's correlation characteristics are improved by time multiplexing BOC (1, 1) and BOC (6, 1) (Figure 4).

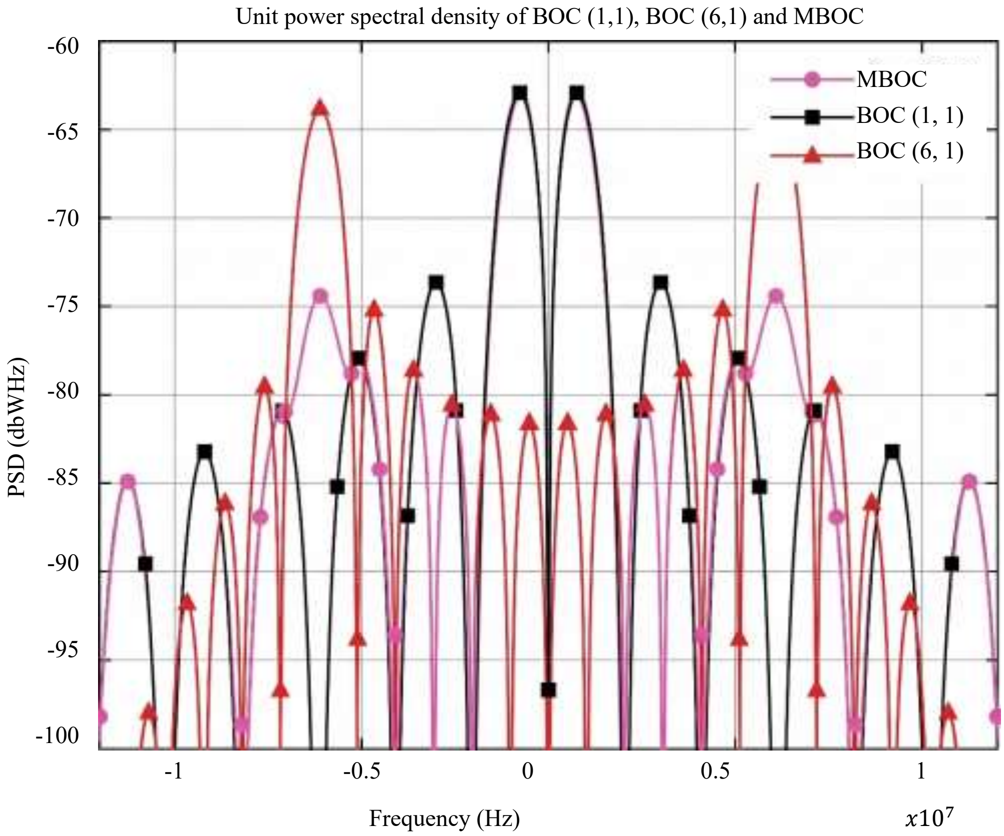

Figure 3. PSD plots of BOC (1, 1) and BOC (6, 1) and MBOC (6, 1, 1/11) [here the frequency center at bottom-axis is considered zero].

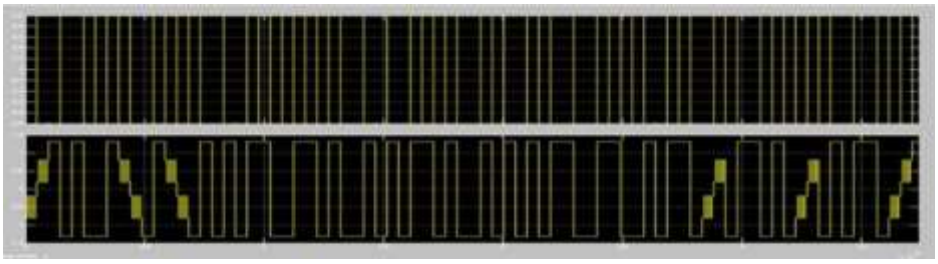

Figure 4: Time domain representation of TMBOC data and pilot signal.

$$G_{pilot}(f) = \frac{29}{33} G_{BOC(1,1)}(f) + \frac{4}{33} G_{BOC(6,1)}(f)$$
$$G_{data}(f) = G_{BOC(1,1)}(f)$$

and for 75–25% distribution

$$G_{\mathrm{MBOC}\left(6,1,\frac{1}{\Pi}\right)}(f) = 0.75 G_{\mathrm{data}}(f) + 0.25 G_{\mathrm{pilot}}(f)$$
$$= \frac{10}{11} G_{\mathrm{BOC}(1,1)}(f) + \frac{1}{11} G_{\mathrm{BOC}(6,1)}(f)$$

Performance Analysis of Modulation Techniques

A BOC signal can be defined as the superposition of two BPSK modulated signals, located at negative and positive sub carriers respectively. BOC modulated signals have a narrower main lobe of their spectrum of auto-correlation function which provides better tracking accuracy (Figure 3).

Because BOC has a higher spectral separation coefficient (SSC) than BPSK signal, it has more multipath mitigation and interference resistance. However, the autocorrelation peaks of signals modulated by MBOC are steeper [50, 51].

It is clear from a detailed examination of the auto-correlation functions of the different MBOC signals. Even though BOC (1,1) is the dominating signal in the MBOC signal, the receiver must still use a false lock detector to ensure that it is monitoring the right autocorrelation main peak and not BOC (1,1)'s secondary lobes. The lower bound of the mean-squared error for estimating a non-random variable is called the Cram'er-Rao lower bound (CRLB). The CRLB defines the ultimate accuracy of any estimation and shows the minimum code pseudo-range variance we would have with the best possible receiver implementation [53]. The CRLB is used to evaluate the performance of the location estimation relies on the delay between the transmitting and receiving signal.

$$CRLB = \frac{B_L}{\frac{C}{N_0}(2\pi)^2 \int_{-\infty}^{\infty} f^2 G_S(f) df} = \frac{B_L}{(C/N_0(\dot{R_{SS}}(0))}$$

For maximum and minimum values of C/N0 of the interest, the theoretical gain in code tracking error decreases with increasing the C/N0 at fixed bandwidth B_L. The BPSK performance is the worst while the CBOC (1/11,'-') shows the best performance (Figure 5). Thus, the theoretical performances of MBOC modulated signals are better than BOC and BPSK modulated signals. Hence, the supremacy of MBOC modulation over BPSK and BOC signal, in terms of interference mitigation and easy detection, is established. After that TMBOC (1/11) shows better tracking accuracy.

Spectrum Allocation Regarding MBOC Modulation

The limited RF spectrum must be designed in such a way that there should be multiple accesses along with available bandwidth, less power consumption, low noise level and high performances of the systems. The modulation technique provides all of these requirements.

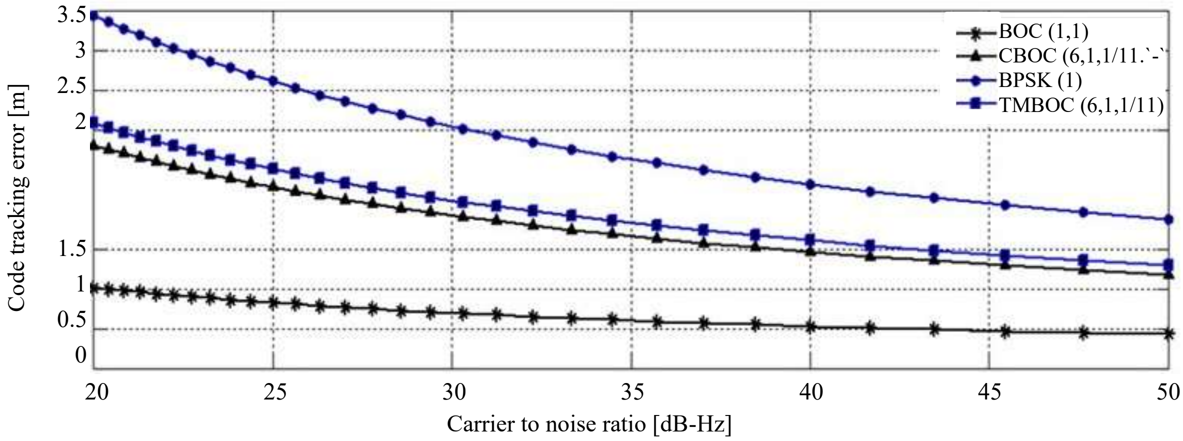

Figure 5. Cram'er Rao Lower Bound with 1 Hz Loop Bandwidth, a 1/12 chip E-L spacing, 4 ms Integration and 12 MHz One-Sided Filter.

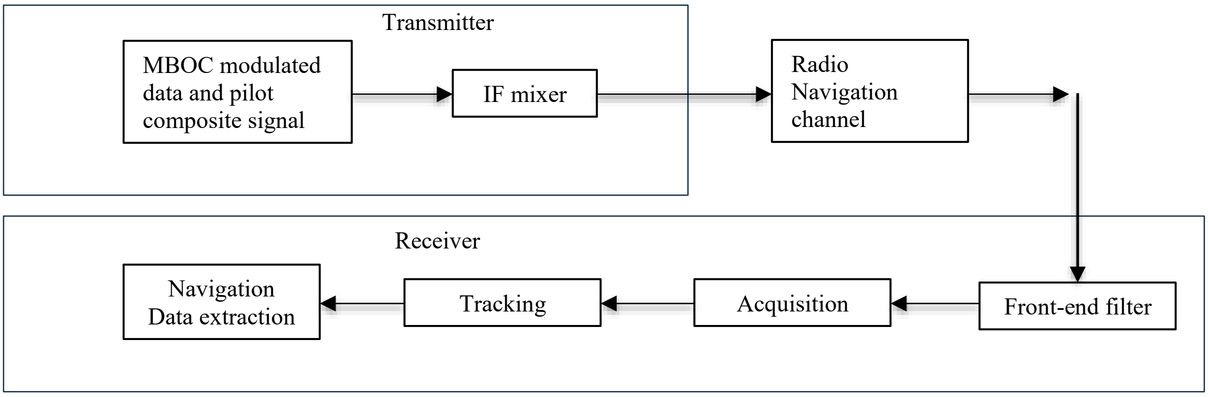

Figure 6. MBOC implemented communication system using IF simulator.

Software Defined Radio (SDR)

A software defined GNSS receiver consists of a front-end filter, Acquisition unit (where identification of PRN code and coarsely estimation of code phase, Doppler frequency are accomplished), Tracking unit (where the received signal are finely tuned with local replica to extract the navigation data) and position determination unit (Figure 6) [55]. SDR can be designed practically and processed by simulation or emulation of the basic modules of a communication system i.e. transmitter section, radio navigation channel section and receiver section. As the whole system is generated using MATLAB software, we consider Intermediate Frequency (IF) simulator for providing our desirable outputs.

In our transmitter model, the MBOC modulation navigation data modulates the carrier signal of 2.5 MHz in cases of narrowband transmitter model and 8.5 MHz carrier signal in cases of wideband transmitter model [54]. After that the IF signal can be converted into L1 band range. Instead of simulating the model of L1 band signal, we transmitted the IF signal through a hostile channel model. But we took care of channel parameters for the analytic signal processing paradigm. The front-end filter of the receiver section limits the bandwidth of received signal. If we replace the RF front-end section of the receiver with the IF section, the simulation becomes easy. Doing this, we can model the channel section such that the correct performance of the receiver can be measured. We mainly give importance to the SDR structure which excludes the RF section.

There are four basic modules in GPS receiver system and they are: a) Front-end filter, b) Acquisition unit (i.e. coarsely finds the Doppler frequency and code phase delay), c) Tracking unit (i.e. finely tuned the received signal to the local PRN code and ready to discard the PRN of received signal) and finally d) Navigation data extraction. The details of above-mentioned units will be described in the subsequent sections.

RESULTS AND DISCUSSION

Specifically created for the GPS L1C signal, the Time Multiplexed Binary Offset Carrier (TMBOC) signal production is a vital component of contemporary Global Navigation Satellite Systems (GNSS). Two Binary Offset Carrier (BOC) signals, BOC (1,1) and BOC (6,1), are intricately combined in TMBOC. The time-multiplexing of these two BOC components, which optimizes the correlation characteristics of the resultant signal, is what makes TMBOC special. The power distribution is a key consideration, and TMBOC adopts a 75-25% distribution, giving precedence to the BOC (1,1) component. Equation 1 delineate the spectral components of the pilot and data channels, respectively, in TMBOC modulation.

The resultant TMBOC signal is characterized by its normalized Power Spectral Density (PSD) (Figure 7). This tailored modulation scheme is specifically designed to enhance tracking precision, mitigate interference, and ensure robust signal reception in GNSS receivers. The broader analysis of modulation techniques, including Direct Sequence Spread Spectrum (DSSS), Binary Phase Shift Keying (BPSK), Binary Offset Carrier (BOC), and Multiplexed Binary Offset Carrier (MBOC), reveals the unique advantages and applications of TMBOC in the context of GNSS signal processing. Additionally, the discussion covers spectrum allocation, software-defined radio (SDR) implementation, and performance metrics such as the spectrum and Cramer-Rao Lower Bound (CRLB), providing a comprehensive overview of the modulation landscape in GNSS systems.

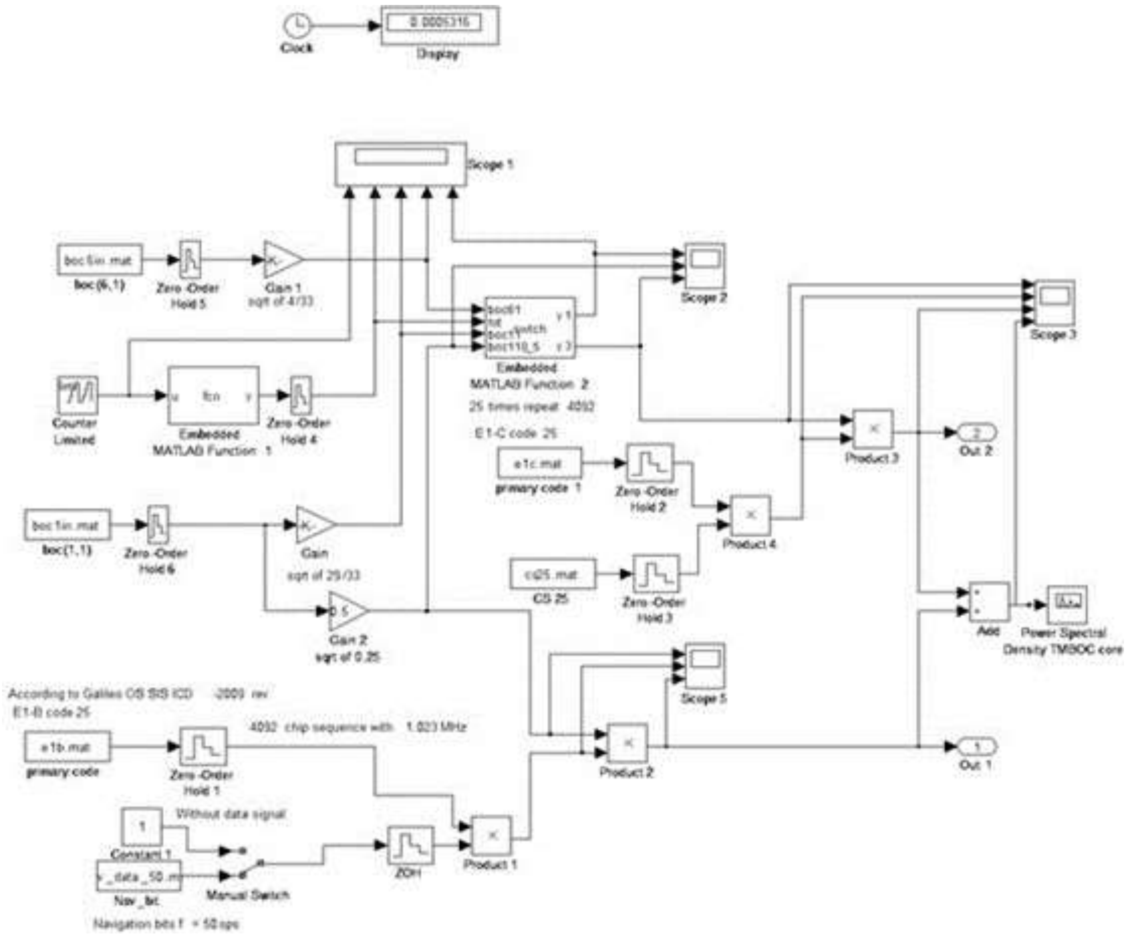

Figure 7. A snapshot of TMBOC signal generation using Simulink.

Code Snippet of the Embedded Function

```
function [y1,y3]= swtch(boc61,hit,boc11,boc110_5) y1=0;
y3=0;
if (hit == 1)
y1 = 0.866025403*boc61;
y3= 0.866025403*boc61 + boc110_5;
elseif (hit==2)
y1=0.866025403*boc11; y3=0.866025403*boc11+ boc110_5;
end;
```

CONCLUSION

This thorough investigation of modulation techniques in the context of Global Navigation Satellite Systems (GNSS) offers insightful knowledge about the variety of signal production and processing techniques used. Time Multiplexed Binary Offset Carrier (TMBOC) signal production, specifically designed for the GPS L1C signal, is emphasized in the analysis. By time-multiplexing the BOC(1,1) and BOC(6,1) components, TMBOC's novel method enhances correlation qualities, highlighting a 75-25% power distribution that favors the BOC(1,1) component.

The broader examination encompassing Direct Sequence Spread Spectrum (DSSS), Binary Phase Shift Keying (BPSK), Binary Offset Carrier (BOC), and Multiplexed Binary Offset Carrier (MBOC) underlines the versatility and distinct advantages of each modulation technique. TMBOC, with its enhanced tracking precision and interference mitigation capabilities, emerges as a promising choice for GNSS applications.

Furthermore, the discussion delves into spectrum allocation strategies, emphasizing the frequency plans and modulations employed by systems like GPS, GNSS, and GALILEO. The software-defined radio (SDR) implementation is recognized for its flexibility in designing and testing GNSS receiver systems.

The performance metrics, including Auto-correlation Function (ACF) and Cram‘er-Rao Lower Bound (CRLB), contribute to a comprehensive understanding of the modulation landscape, guiding the ongoing advancements in GNSS technology. In essence, this exploration not only sheds light on TMBOC's pivotal role but also provides a holistic overview of modulation techniques crucial for the evolution and optimization of GNSS systems.

Various approaches that have been surveyed in this paper for estimation of forest height using Pol-InSAR data are RVoG Random Volume over Ground model, Elevated Random Volume over Ground model ERVoG, and Oriented Volume over Ground model OVoG. The use of Light Detection and Ranging (LiDAR), which has been the current state of the art in the studies, gives an accurate estimation of forest height. We also discussed the application of Pol-InSAR in scattering features. We plan to develop and do a detailed analysis and study of Pol-InSAR in the future.

Acknowledgement

The authors are thankful to Dr. Tapan Misra and Dr. Arundhati MisraRay SAC, ISRO for valuable suggestion. Authors are also thankful to Dr. Amitabha Bhattacharya from IIT Kharagpur for his guiding throughout the project completion.

REFERENCE

1. Rabus B, Eineder M, Roth A, Bamler R. The shuttle radar topography mission—a new class of digital elevation models acquired by spaceborne radar. ISPRS journal of photogrammetry and remote sensing. 2003 Feb 1;57(4):241-62.

2. Rossi C, Gonzalez FR, Fritz T, Yague-Martinez N, Eineder M. TanDEM-X calibrated raw DEM generation. ISPRS Journal of Photogrammetry and Remote Sensing. 2012 Sep 1;73:12-20.
3. Treuhaft RN, Moghaddam M, van Zyl JJ. Vegetation characteristics and underlying topography from interferometric radar. Radio science. 1996 Nov;31(6):1449-85.
4. Treuhaft RN, Siqueira PR. Vertical structure of vegetated land surfaces from interferometric and polarimetric radar. Radio science. 2000 Jan;35(1):141-77.
5. Bamler R, Hartl P. Synthetic aperture radar interferometry. Inverse problems. 1998 Aug 1;14(4):R1-54.
6. Li M. Z., H. J. Guo, W. Y. Fan, and Z. Zhen, “Remote sensing analysis of forest site quality in Daxing’an mountain based on GWR,” Scientia Silvae Sinicae, June 2017, vol. 53, pp. 56-66. M. Young, The Technical Writer’s Handbook. Mill Valley, CA: University Science, 1989.
7. Reza M, Amir MM, Imran M, Pandey G, Camponeschi F, Maresca S, Scotti F, Serafino G, Malacarne A, Porzi C, Ghelfi P. Multi-static multi-band synthetic aperture radar (SAR) constellation based on integrated photonic circuits. Electronics. 2022 Dec 12;11(24):4151.
8. Cloude SR, Papathanassiou KP. Polarimetric SAR interferometry. IEEE Transactions on geoscience and remote sensing. 1998 Sep 30;36(5):1551-65.
9. Brandfass M, Hofmann C, Mura JC, Papathanassiou KP. Polarimetric SAR interferometry as applied to fully polarimetric rain forest data. InIGARSS 2001. Scanning the Present and Resolving the Future. Proceedings. IEEE 2001 International Geoscience and Remote Sensing Symposium (Cat. No. 01CH37217) 2001 Jul 9 (Vol. 6, pp. 2575-2577). IEEE.
10. Yamada H, Sato K, Yamaguchi Y, Boerner WM. Interferometric phase and coherence of forest estimated by ESPRIT-based polarimetric SAR interferometry. InIEEE International Geoscience and Remote Sensing Symposium 2002 Jun 24 (Vol. 2, pp. 829-831). IEEE.
11. Brandfass M. Generation of bald Earth digital elevation models as applied to polarimetric SAR interferometry. InIEEE International Geoscience and Remote Sensing Symposium 2002 Jun 24 (Vol. 2, pp. 1014-1016). IEEE.
12. Tao X, Jian Y, Yingning P. A new approach for DEM generation based on polarimetric SAR interferometry. In2006 CIE International Conference on Radar 2006 Oct 16 (pp. 1-4). IEEE.
13. Ferro-Famil L, Pottier E, Lee JS. Unsupervised classification and analysis of natural scenes from polarimetric interferometric SAR data. InIGARSS 2001. Scanning the Present and Resolving the Future. Proceedings. IEEE 2001 International Geoscience and Remote Sensing Symposium (Cat. No. 01CH37217) 2001 Jul 9 (Vol. 6, pp. 2715-2717). IEEE.
14. Xu L, Li S, Deng Y, Wang R. Unsupervised classification of polarimetric synthetic aperture radar interferometry using polarimetric interferometric similarity parameters and SPAN. IET Radar, Sonar & Navigation. 2014 Dec;8(9):1135-44.
15. Boerner WM. Recent advances in extra-wide-band polarimetry, interferometry and polarimetric interferometry in synthetic aperture remote sensing and its applications. IEE Proceedings-Radar, Sonar and Navigation. 2003 Jun 2;150(3):113-24.
16. Shen P, Wang C, Luo X, Fu H, Zhu J. PolInSAR complex coherence nonlocal estimation using shape-adaptive patches matching and trace-moment-based NLRB estimator. IEEE Transactions on Geoscience and Remote Sensing. 2020 May 19;59(1):260-72.
17. Shimada T, Natsuaki R, Hirose A. Pixel-by-pixel scattering mechanism vector optimization in high-resolution PolInSAR. IEEE Transactions on Geoscience and Remote Sensing. 2018 Jan 18;56(5):2587-96.
18. Dubois-Fernandez P, Dupuis X, Garestier F. POLINSAR calibration of a single-pass deramp-on–receive system: example of RAMSES airborne radar. Canadian Journal of Remote sensing. 2005 Jan 1;31(1):112-21..
19. Cloude SR, Papathanassiou KP. Three-stage inversion process for polarimetric SAR interferometry. IEE Proceedings-Radar, Sonar and Navigation. 2003 Jun 2;150(3):125-34.
20. Treuhaft RN, Cloude SR. The structure of oriented vegetation from polarimetric interferometry. IEEE Transactions on geoscience and remote sensing. 2002 Aug 6;37(5):2620-4.
21. Le Toan T, Quegan S, Davidson MW, Balzter H, Paillou P, Papathanassiou K, Plummer S, Rocca F, Saatchi S, Shugart H, Ulander L. The BIOMASS mission: Mapping global forest biomass to

better understand the terrestrial carbon cycle. Remote sensing of environment. 2011 Nov 15;115(11):2850-60.
22. Reiche J, Lucas R, Mitchell AL, Verbesselt J, Hoekman DH, Haarpaintner J, Kellndorfer JM, Rosenqvist A, Lehmann EA, Woodcock CE, Seifert FM. Combining satellite data for better tropical forest monitoring. Nature Climate Change. 2016 Feb;6(2):120-2.
23. Krieger G, Hajnsek I, Papathanassiou K, Eineder M, Younis M, De Zan F, Prats P, Huber S, Werner M, Fiedler H, Freeman A. The tandem-L mission proposal: Monitoring earth's dynamics with high resolution SAR interferometry. In2009 IEEE Radar Conference 2009 May 4 (pp. 1-6). IEEE.
24. Deng L, Yan YN, Wang C. Improved POLSAR image classification by the use of multi-feature combination. Remote Sensing. 2015 Apr 8;7(4):4157-77.
25. Ramya MN, Kumar S. PolInSAR coherence-based decomposition modeling for scattering characterization: A case study in Uttarakhand, India. Science of Remote Sensing. 2021 Jun 1;3:100020.
26. Shafai SS, Kumar S. PolInSAR coherence and entropy-based hybrid decomposition model. Earth and Space Science. 2020 Oct;7(10):e2020EA001279.
27. Garestier F, Dubois-Fernandez P, Dupuis X, Paillou P, Hajnsek I. PolInSAR analysis of X-band data over vegetated and urban areas. IEEE Transactions on Geoscience and Remote Sensing. 2006 Jan 23;44(2):356-64.
28. Santoro M, Askne J, Dammert PB. Tree height estimation from multi-temporal ERS SAR interferometric phase. InProceeding of FRINGE 2003 Workshop 2003 Dec (pp. 1-5).
29. Renaudin E, Mercer B, Zhang Q, Collins MJ. Biomass Estimation Using Vertical Forest Structure from SAR Tomograghy: a Case Study in Canadian Boreal Forest. The International Archives of the Photogrammetry, Remote Sensing and Spatial Information Sciences. 2012 Jul 30;39:431-5.
30. Lee JS, Grunes MR, De Grandi G. Polarimetric SAR speckle filtering and its implication for classification. IEEE Transactions on Geoscience and remote sensing. 1999 Sep 30;37(5):2363-73.
31. Lee JS, Grunes MR, Ainsworth TL, Schuler DL, Cloude SR. Coherence estimation and speckle filtering based on scattering properties. InIGARSS 2003. 2003 IEEE International Geoscience and Remote Sensing Symposium. Proceedings (IEEE Cat. No. 03CH37477) 2003 Jul 21 (Vol. 2, pp. 705-707). IEEE.
32. Chen SW, Wang XS, Sato M. PolInSAR complex coherence estimation based on covariance matrix similarity test. IEEE Transactions on Geoscience and Remote Sensing. 2012 May 4;50(11):4699-710.
33. Pritt MD. Two-dimensional phase unwrapping: theory, algorithms, and software. Wiley; 1998.
34. Costantini M. A novel phase unwrapping method based on network programming. IEEE Transactions on geoscience and remote sensing. 2002 Aug 6;36(3):813-21.
35. Pepe A, Lanari R. On the extension of the minimum cost flow algorithm for phase unwrapping of multitemporal differential SAR interferograms. IEEE Transactions on Geoscience and remote sensing. 2006 Aug 21;44(9):2374-83.
36. Goldstein RM, Werner CL. Radar interferogram filtering for geophysical applications. Geophysical research letters. 1998 Nov 1;25(21):4035-8.
37. Huang H, Wang Q. A method of filtering and unwrapping SAR interferometric phase based on nonlinear phase model. Progress In Electromagnetics Research. 2014;144:67-78.
38. Natsuaki R, Hirose A. SPEC method—A fine coregistration method for SAR interferometry. IEEE transactions on geoscience and remote sensing. 2010 Aug 23;49(1):28-37.
39. Sansosti E, Berardino P, Manunta M, Serafino F, Fornaro G. Geometrical SAR image registration. IEEE Transactions on Geoscience and Remote Sensing. 2006 Sep 25;44(10):2861-70.
40. Zhou W, Chen E, Liu G, Li W, Feng Q, Wang X. Polarimetric interferometic coherence optimization-based DEM extraction method for ALOS PALSAR data. In2012 IEEE International Geoscience and Remote Sensing Symposium 2012 Jul 22 (pp. 2691-2694). IEEE.
41. Salembier P, Garrido L. Binary partition tree as an efficient representation for image processing, segmentation, and information retrieval. IEEE transactions on Image Processing. 2000 Apr 30;9(4):561-76.

42. Zebker HA, Van Zyl JJ. Imaging radar polarimetry: A review. Proceedings of the IEEE. 1991 Nov 30;79(11):1583-606.
43. Lee JS, Grunes MR, Kwok R. Classification of multi-look polarimetric SAR imagery based on complex Wishart distribution. International Journal of Remote Sensing. 1994 Jul 20;15(11):2299-311.
44. Papathanassiou KP, Cloude SR. Single-baseline polarimetric SAR interferometry. IEEE Transactions on Geoscience and Remote Sensing. 2002 Aug 6;39(11):2352-63.
45. Garestier F, Dubois-Fernandez PC, Champion I. Forest height inversion using high-resolution P-band Pol-InSAR data. IEEE Transactions on Geoscience and Remote Sensing. 2008 Nov 21;46(11):3544-59.
46. Fu H, Zhu J, Wang C, Wang H, Zhao R. Underlying topography estimation over forest areas using high-resolution P-band single-baseline PolInSAR data. Remote Sensing. 2017 Apr 12;9(4):363.
47. Zou B, Cai H, Zhang L, Lin M. Model of man-made target beneath foliage using polinsar. Progress In Electromagnetics Research Letters. 2008;2:21-8.
48. Lopez-Martinez C, Papathanassiou KP. Cancellation of scattering mechanisms in PolInSAR: Application to underlying topography estimation. IEEE Transactions on Geoscience and remote sensing. 2012 Aug 2;51(2):953-65.
49. Hein GW, Avila-Rodriguez JA, Wallner S, Pratt AR, Owen J, Issler JL, Betz JW, Hegarty CJ, Lenahan S, Rushanan JJ, Kraay AL. MBOC: the new optimized spreading modulation recommended for GALILEO L1 OS and GPS L1C. InProceedings of IEEE/ION PLANS 2006 2006 Apr 27 (pp. 883-892).
50. Progri IF, Bromberg MC, Michalson WR, Wang J. A theoretical survey of the spreading modulation of the new GPS signals (L1C, L2C, and L5). InProceedings of the 2007 National Technical Meeting of The Institute of Navigation 2007 Jan 24 (pp. 561-569).
51. Ávila Rodríguez JÁ. On generalized signal waveforms for satellite navigation (Doctoral dissertation, München, Univ. der Bundeswehr, Diss., 2008).
52. Progri IF. On generalized multidimensional geolocation modulation waveforms. InProceedings of the 2012 IEEE/ION Position, Location and Navigation Symposium 2012 Apr 23 (pp. 919-951). IEEE.
53. Avila-Rodriguez JA, Wallner S, Hein G, Rebeyrol E, Julien O, Macabiau C, Ries L, DeLatour A, Lestarquit L, Issler JL. CBOC: an implementation of MBOC. InCNES-ESA, 1st Workshop on GALILEO signals and Signal Processing 2006 Oct 12.
54. Siddiqui BA, Zhang J, Bhuiyan MZ, Lohan ES. Joint data-pilot acquisition and tracking of Galileo E1 open service signal. In2010 Ubiquitous Positioning Indoor Navigation and Location Based Service 2010 Oct 14 (pp. 1-7). IEEE.
55. Ashby N. Relativity in the global positioning system. Living Reviews in relativity. 2003 Dec;6(1):1-42.
56. Weiler RM, Blunt P, Hodgart S, Unwin M. The effect of cosine phased BOC modulation on the GNSS receiver search process. The Journal of Navigation. 2008 Oct;61(4):591-611.

